# Wellhead-based Casing Integrity Assessment and Monitoring

**Yuxin Wu[1], Jiannan Wang[1], Mike Wilt[1], Evan Um[1], Chester Weiss[2], Donald Vasco[1]**

**[1]Lawrence Berkeley National Laboratory**

**[2]Sandia National Laboratories**

**Keywords**

*Wellhead, Casing Integrity, Electromagnetism, Time-Domain Reflectometry, Tube Wave*

## ABSTRACT

Wellbores provide subsurface access for resource extraction, storage and waste disposal. They are often challenged by complex and aggressive mechanical and geochemical conditions, affecting their integrity, efficiency and reliability. This is exacerbated in geothermal fields due to the extreme temperature conditions at depth, repeated thermal cycling, fluid manipulation and the presence of corrosive chemicals. Wellbore integrity is of paramount importance to safe and effective geothermal energy extraction.

Assessments for wellbore integrity relies almost entirely on downhole logging tools currently. Such tools typically require borehole occupation which interrupts the operation of the wells. Because of the relatively high cost, these measurements are only performed occasionally, typically when problems are suspected, limiting their usefulness for borehole degradation trajectory prediction for potential failure warning.

We developed and tested a new generation of borehole monitoring tools using only wellhead based approaches. These approaches are (1) non-intrusive and does not require behind-casing or in-casing sensor installation or deployment; (2) cost effective, which allows frequent monitoring of the well during its life cycle; and (3) fast and easy to use, which facilitates its better acceptance and application by regular customers. Our approach integrates transient and steady state electromagnetism (EM), tubular seismic wave propagation and electrochemical sensing. Specifically, steady state EM and electrochemical sensing can provide fast and low cost casing integrity screening, and guided transient EM and tubular seismic wave sensing can provide higher precision targeting of wellbore irregularity in geothermal wells.

Both experimental and numerical experiments were conducted at both laboratory and field scales, and our results demonstrated the sensitivities of these approaches to casing length and damage induced geophysical anomalies. These results revealed the potential of these approaches

which could lead to a new set of non-invasive, fast and economic tools for borehole integrity accessed in geothermal as well as other subsurface applications.

## 1. Introduction

Wellbores provide subsurface access for resource extraction, storage and waste disposal. They are often challenged by complex and aggressive mechanical and geochemical conditions, affecting their integrity, efficiency and reliability. This is exacerbated in geothermal fields due to the extreme temperature conditions at depth, repeated thermal cycling, fluid manipulation and the presence of corrosive chemicals in the fluids.

Damages to wellbores vary significantly in rate, pattern and depth depending on the thermal, hydrological, mechanical and chemical conditions of specific reservoirs. Assessment for wellbore integrity relies almost entirely on downhole logging tools currently. Such tools typically require borehole occupation which interrupts the operation of the wells. Because of the relatively high cost, these measurements are only performed occasionally, typically when problems are suspected, limiting their usefulness for borehole degradation trajectory prediction for potential failure warning.

A new generation of advanced borehole monitoring tools is critically needed to improve the current state of wellbore integrity assessment. Ideally, these new tools should be: (1) non-intrusive, which does not require behind-casing or in-casing sensor installation or deployment, thus minimizing the potential risk of introducing new leakage pathways or interrupting the normal operation of the wells; (2) cost effective, which allows frequent monitoring of the well during its life cycle in order to help understand degradation trajectory and provide early warning before potential failure; and (3) fast and easy to use, which facilitates its better acceptance and application by regular customers.

## 2. Technical Background

We are developing an integrated suite of technologies combining electromagnetism, seismic tube wave and electrochemical methods for non-invasive monitoring and assessment of borehole integrated based on wellhead deployment (Figure 1). While this presentation will primarily focus on EM and seismic methods, our electrochemical studies have yield novel results regarding corrosion estimations in geothermal wells under relevant geochemical conditions at up to 240 °C.

Here we provide brief discussions of the technological background on the EM and seismic technologies and identify the key challenges facing their applications for subsurface wellbore integrity assessment.

### *2.1 Low frequency EM imaging*

Casing damages change its impedance along the length. As a result, the path of an injected electrical current and the induced external electrical field, measureable from the surface, will be

altered. This suggests a possible method to detect casing damage by analyzing the electrical field generated by an energized casing. This can be carried out by applying electrical sources on the wellhead, and analyzing its electrical field on the surface.

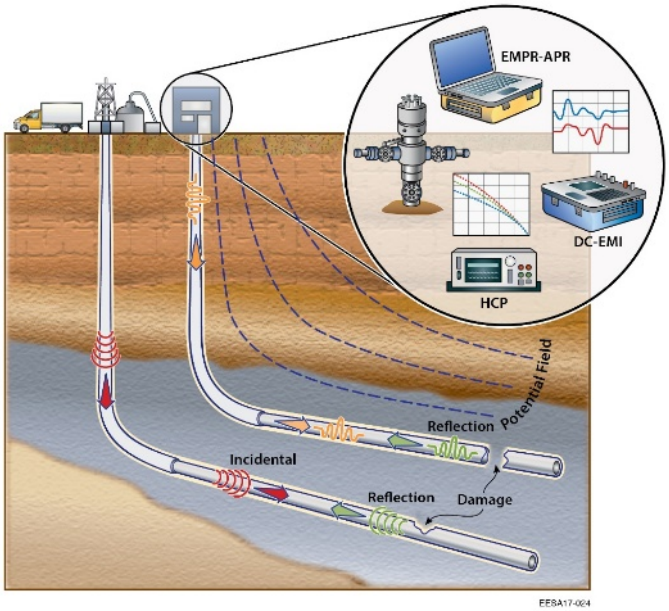


**Figure 1: Schematics of casing-based wellbore integrity monitoring concept with EM, tube wave and electrochemical sensing (Wilt et al, 2018).**

For a DC, or low frequency, electrical current source applied at the wellhead with a distant return, the electrical current along the casing in a homogeneous earth can be represented by the following equation (Kaufman, 1990).

$$I_{cas}(z) = I_0 \exp\left(-\frac{z}{L_c}\right) \quad \text{Where} \quad L_c = \sqrt{\rho_{formation}\sigma_{case}A_{case}} \qquad (1)$$

Here, $I_o$ is the source current, $z$ is the depth down the casing, and $L_c$ is the conduction length, or the length where the current has diminished by 1/e due to leak-off (Schenkel and Morrison, 1990). $L_c$ is approximated in the zone near the source injection point by the square root of the product of the casing conductivity ($\sigma_{case}$), its cross-sectional area ($A_{\text{case}}$), and the formation resistivity ($\rho_{formation}$). In general, for soft iron steel casings that is typically used for deep boreholes the conduction length varies from 200 m to more than 2 km, depending on the number of casing strings, the casing properties, and the background resistivity. This suggests that for most wells sufficient current can be injected to distinguish between completions with variable depths and configurations. Numerical codes to simulate casing response to current excitation for realistic models have been developed by several groups. Cylindrically symmetric codes, which are suitable for isolated vertical wells, are readily available (Schenkel and Morrison, 1994). Deviated well trajectories with complex background and higher frequency computations require

3D codes, which have been developed at LBNL (e.g. Commer et al., 2015; Um et al., 2015). A new DC model that allows for multiple casing strings as well as surface piping is developed by Weiss and can be used (Weiss, 2017).

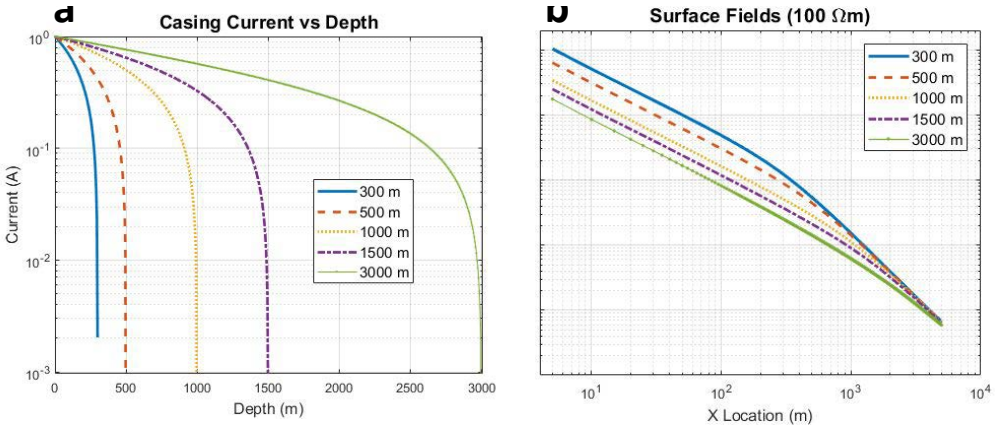


**Figure 2: a. Electric current distribution along the well casing when its wellhead is excited with a surface electric pole source (distant return electrode); b. Surface electrical profile from the wellbores. Five different casing lengths (300, 500, 1000, 1500 and 3000m) are considered (Figures modified from Wilt et al, 2019).**

Figure 2 illustrates the concept of the method by showing the electrical current profile along the casing (Figure. 2a), and the surface electrical potential decay curves from different lengths of casings (Figure. 2b), illustrating the sensitivity of the method. The casing conductivity is set at 5.5E6 S/m with a distant return electrode and a uniform 100 ohm-m half space resistivity. For a broken casing, the potential field strongly resembles that from a shorter section above the break; for a corroded casing the field is between the full-length casing and the broken casing, depending on the severity of the corrosion.

### *2.2 EM and seismic pulse reflectometry*

Electromagnetism based Time Domain Reflectometry (TDR) are used in the electric and electronics industry for fault location on power or signal delivering cables (Furse et al., 2009; Amir et al., 2010), or in the earth science field for soil moisture estimation (Ledieu et al, 1986). It operates by sending a coded short pulse of source signal down the wire/pipe and measures the reflected signal off impedance anomalies caused by damages or short circuiting. The characteristics of the reflection (e.g. travel time, shape, polarity and magnitude) is proportional to the distance to and the damage severity of the faults. Opposite to the low frequency EM method discussed above that relies on the leak-off current from the casing, reflectometry method senses the electrical signal confined on the casing itself. The characteristics of the incidental signal can be tailored toward a specific application, e.g. live wire testing, to improve signal to noise ratio (SNR) or reduce interference with the indigenous signals the wires are carrying.

The reflection coefficient ($\Gamma$) gives a measure of the signal return and is defined by

$$\Gamma = \frac{V_{reflected}}{V_{incident}} = \frac{Z_d - Z_0}{Z_d + Z_0} \quad (2)$$

Where $Z_0$ is the characteristic impedance of the wire and $Z_d$ is the impedance of the discontinuity (Iskander, 1992). As such, the reflection coefficient is 1 for an open circuit ($Z_d$ = infinity), and -1 for a short circuit ($Z_d$ = 0), and they are shown as positive and negative return signals on the recorded trace as demonstrated in Figure 3.

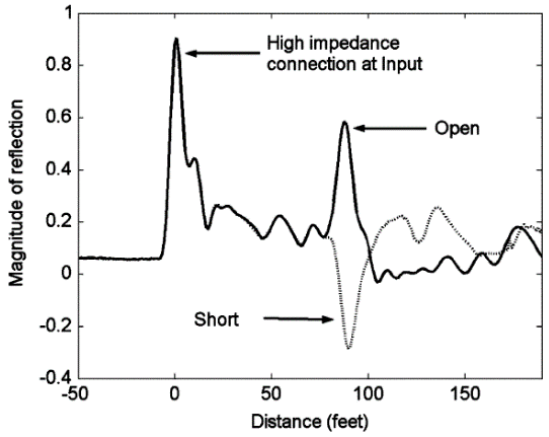


**Figure 3: Example of reflectometry signals from open and short circuits (modified from Furse et al., 2009).**

A round-trip travel time of the EM signal is used to calculate the distance to damage based on a characteristic velocity $V_p$. $V_p$ is typically a fraction of the speed of light (3E8 m/s), determined by the dielectric properties of the signal carrying conductors and the surrounding material, e.g. concrete cement or oil mud. For its application in subsurface wellbore integrity monitoring, the steel casing conductor can guide the propagation of EM signals initiated from the wellhead. Damages to casing due to corrosion or stress can lead to changes of its impedance, generating a reflected signal, coded with the information of the damage. The physics of the reflectometry technology is well studied and its potential for wellbore integrity monitoring is significant.

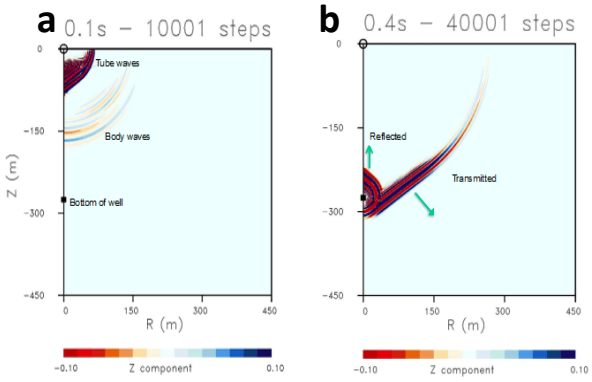


**Figure 4: a. body and tube waves 0.1 s after exciting a seismic wave at the surface; b. Reflected and transmitted tube waves 0.4 s after the initiation of the seismic source. These results were computed using LBL's cylindrical symmetric finite difference code.**

Similar to EM, seismic reflectometry is based on similar principles and uses the seismic tube wave traveling along the casing for subsurface diagnosis. Often considered noise in borehole seismic surveys, the properties of seismic tube waves are sensitive to wellbore damages due to stress or corrosion (Alexandrov et al., 2007). Previous studies have modeled tube wave propagation along casing (Figure 4) and its sensitivity to casing corrosion and fractures (Alexandrov et al., 2007; Ponomarenko, 2008). Experimental studies for such applications have been very limited.

## 3. Results and Discussion

The goal of this research is to demonstrate the proof-of-concept feasibility of the suite of technologies discussed above for borehole integrity monitoring based on wellhead deployment. Toward this goal, we have conducted a series of numerical and experimental studies at both laboratory and field scales for each of the technologies presented above. We will briefly discuss each of the technologies below.

### *3.1 Low frequency EM*

Using the code developed by Um et al (2015) and Weiss (2017), numerical experiments have been conducted to simulate 3D distribution of the potential fields when the wellbore is energized at the wellhead. Results from a numerical experiment is shown in Figure 5 below.

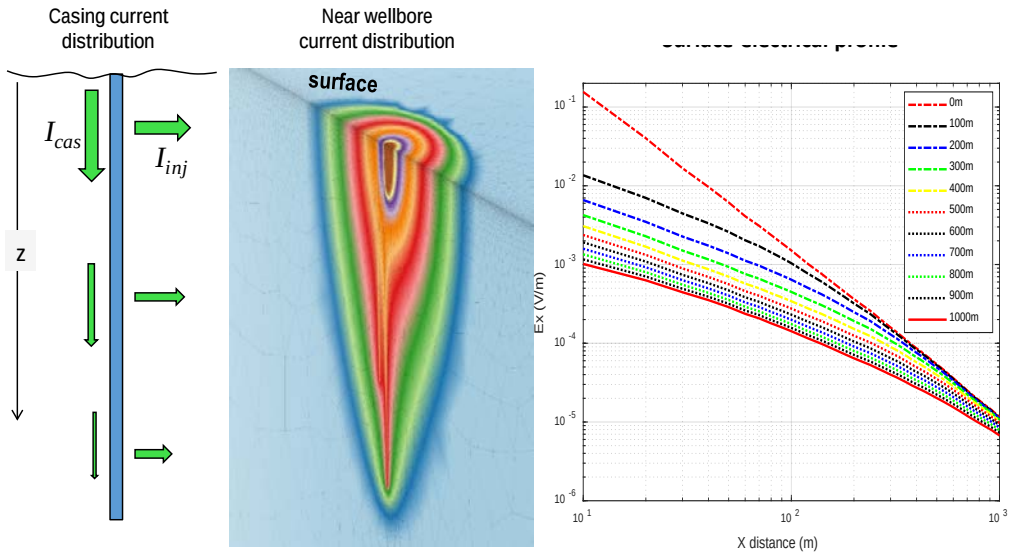


**Figure 5: a. Current profile along the casing; b. Electrical potential field decay with distance away from the casing observed on the surface.**

Figure 5a shows the conceptual distribution of the electrical current along the borehole when energized at the wellhead. Decreasing of the current density with depth is primarily dictated by the formation resistivity that impacts the magnitude of current leakage into formations. Figure 5b illustrates simulated 3D potential distribution near the borehole in a homogenous media that

visualizes the decay of the potential field with depth. Figure 5c shows a set of simulations with different borehole lengths indicating the sensitivity of this approach. A severely damaged borehole can be treated as a borehole shortened at the point of damage, and would thus have a shift of this potential field profiles measured at the surface. While results not shown, partially damaged borehole simulations have also been conducted, and showed sensitivity based on surface measurements as well (Wilt et al., 2018).

Experiments at field scales have been conducted at multiple locations. Comparison between these experimental results and numerical simulations suggests good agreement between the measurements and the models. An example from the Containment and Monitoring Institute (CaMI) site in Alberta Canada is shown below in Figure 6. Figure 6a shows the layout of the field site with the position of the two observational wells (OBS1, OBS2) and the injection wells for $CO_2$. EM monitoring was conducted for OBS1/OBS2 wells along a linear transect across these wells indicated by the red, dashed line. Figure 6b and 6c show the comparison between the simulated results (solid line) and the measurements (circles) for both wells, and an excellent agreement can be observed between these two datasets. Note that because OBS2 is much shallower than OBS1, a much higher magnitude of potential field was observed. Additional tests using data from central Texas, California and other locations all indicated similar performance of the methods in wells with large variations of depths and conditions, indicating the versatility of this approach for borehole monitoring.

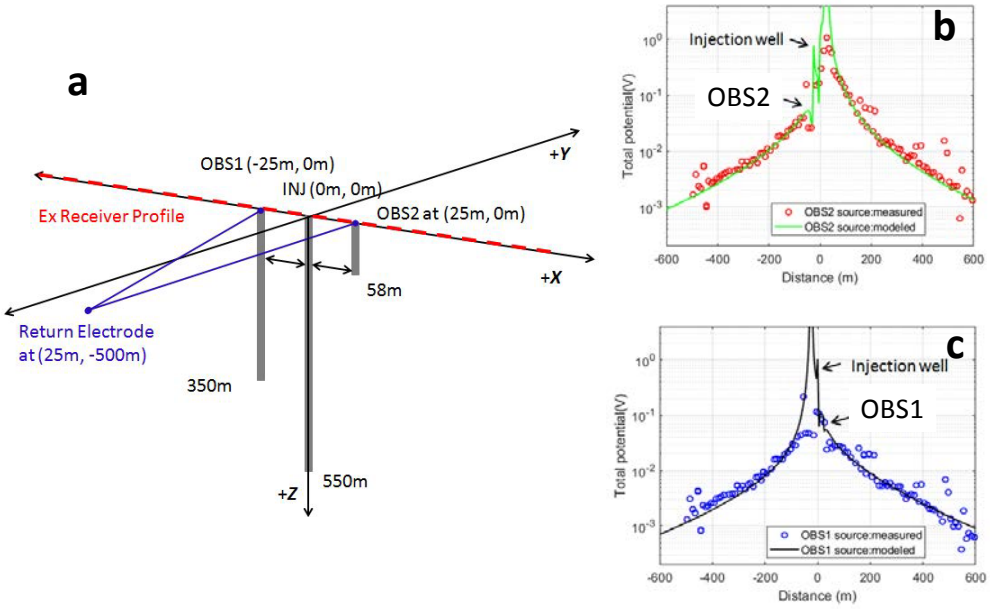


**Figure 6: a. Data acquisition layout at CaMI showing the position of the OBS wells, data transect and the return electrode positon; b/c. Comparison between observed data and numerical modeling results for OBS1 and OBS2 wells.**

In addition to the studies discussed above where only a single well is simulated, we also simulated EM response from large fields with many existing wells and pipeline infrastructures using the numerical capabilities developed by Weiss (Weiss, 2017). Simulation results show that the presence of steel wells and infrastructure have a significant impact on the electrical field distribution on the surface and neglecting these boreholes and pipelines can introduce significant

error to data interpretation. On top of these factors, other key factors that impact the signal include borehole structure, e.g. surface casing presence/properties, borehole material properties amongst others. Our numerical studies have explored the impact of these factors and quantified their effects.

### *3.2 EM Reflectometry*

The electrical behavior of the casing under the excitation of a short time domain signal was simulated with a two-step model. First, we simulate the cross-section of the wellbore using the finite difference method (FDM). The model of the cross-section is conducted under a few scenarios, including intact well-bore, casing-only damaged, and both casing and outer cementation damage. We calculate the characteristic impedance from the cross-sections using:

$$Z = \sqrt{\frac{L}{C}} = \sqrt{\frac{LC_0}{CC_0}} = \frac{1}{v_0\sqrt{CC_0}}, \#(3)$$

Where $C$ is the capacitance per unit length of the model. $C_0$ is the capacitance per unit length in the absence of any dielectric media (cementation and surrounding geologic formation). $L$ is the inductance. $v_0$ is the electromagnetic wave velocity in the vacuum. Here, the capacitance ($C$) can be calculated from:

$$C = \frac{q}{V_0}, \#(4)$$

$$q = \epsilon_0 \oint \epsilon_r(x,y)E(x,y), \#(5)$$

Where $V_0$ is the excitation voltage, which is arbitrarily defined as a boundary condition, and can be simply fixed at a normalized value as 1.0 V. $\varepsilon_0$ is the permittivity of the free space. $\varepsilon_r$ is the relative permittivity. $E$ is the electric field and $q$ is the total charge per unit length. We can calculate $q$ by Gauss's law in Equation 5. The close surface can be in any shape, provided the surface encloses the inner casing. In this paper, we use the cubic square as the close surface. At last, we incorporate the characteristic impedance into the 1D model along the longitudinal ($z$) direction of the well, which only considers the overall reflectometry response.

Our initial model test was conducted on coaxial cable, which is the ideal model where each of the components presents in the model is homogeneous and spatially continuous. In addition, the outer insulation of the cable is nearly perfect, thus no current leak-off is possible unless the cable is damaged. Figure 7 shows the coaxial cable under investigation as well as the numerical simulations under both undamaged and damaged scenarios.

As shown in Figure 7a, the inner conductor and the metallic sheath complete the signal pathways and the dielectric material in between provides the isolation. The analogy to this model in subsurface boreholes would be the multilayers of casings with cements in between. Figure 7b/7c shows the modeled cross section with assigned dielectric properties and the simulated electrical potential field at the cross section for undamaged cable. As expected, the gradient of the potential field radiates away from the center conductor in the dielectric material with no gradient inside the central conductor in any directions. Comparison between the damaged (Fib. 7d/7e) with the undamaged model shows the biased dispersion of the potential field toward the direction of the damage which results in leakage of electrical currents. These two cases present contrasting

dielectric behavior in the cross-section plat which, when modeled into a 1D model into the *z* direction, will lead to very different attenuation/dispersion behaviors.

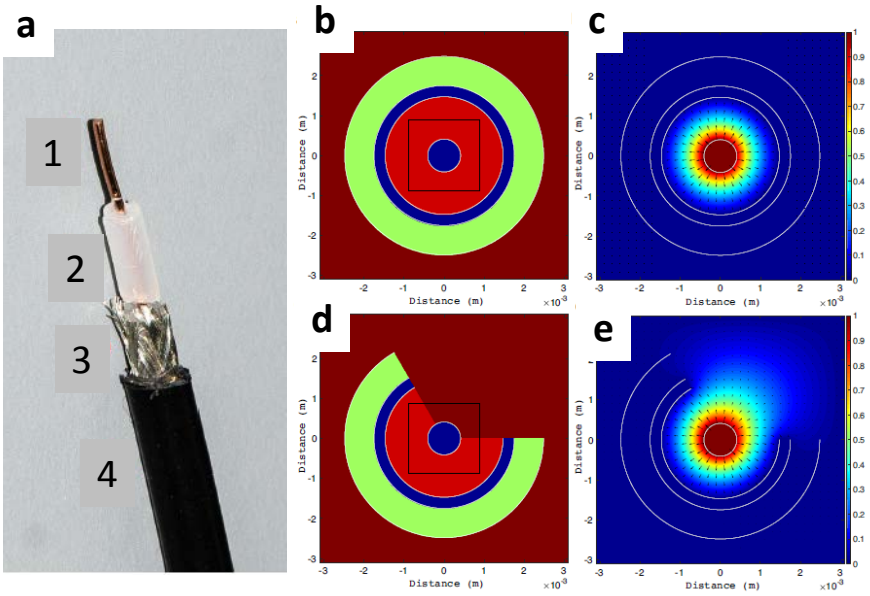


**Figure 7: a. The model coaxial cable cutaway. 1 is the copper conductor. 2 is the inner dielectric insulator. 3 is the metallic shield. 4 is the outer plastic sheath; b. Numerical model of the undamaged coaxial cable. The light green is the outmost PVC shield. The blue represents the inner conductor and metal jacket. Red is the dielectric insulation layer. The black box in the middle is the contour for the Gauss integration in Equation 5; c. Normalized voltage potential field. The black arrows represent electric field direction; d. Numerical model of the damaged coaxial cable with 120° cut-away; e. Normalized voltage potential field. The black arrows represent electric field direction.**

Extending the 2D model presented above into the third dimension, the reflectometry behavior of the electrical signal is simulated and compared with experimental observations. These results are shown in Figure 8. Figure 8a shows the numerical simulation of the propagating signals in both undamaged and damaged cases, and Figure 8b shows the experiment results of the same scenarios. Comparison of these results shows excellent agreement between the model and the data. Note that the damage made to the cable was at the middle of the cable, therefore the observed new peak (shown as red) with the opposite polarization in both the model and the data. These datasets validate the experimental and numerical methods for its further testing in more complicated scenarios.

A series of tests with increasing complexity were conducted after the initial tests with coaxial cables, each validating the methods. Here we only present one testing case at field scale using an existing wellbore in the central value region (Figure 9). Note that while this is an oil and gas well, the bottom temperature of the well is roughly at ~ 260 °C due to long term steam injection. This sets up a thermal condition similar to geothermal wells in addition to borehole construction similarities. The wellbore is about 800 ft. deep with multiple casing strings (Figure 9a/9b). Figure 9c/9d/9e showed numerical simulation of the electrical behavior of the multi-casing string at the cross section, indicating the zone of impact extending all the way to the surface casing

layer. This suggests current leakage into the formation during signal propagation which is different from ideal cases with the co-axial cable presented above.

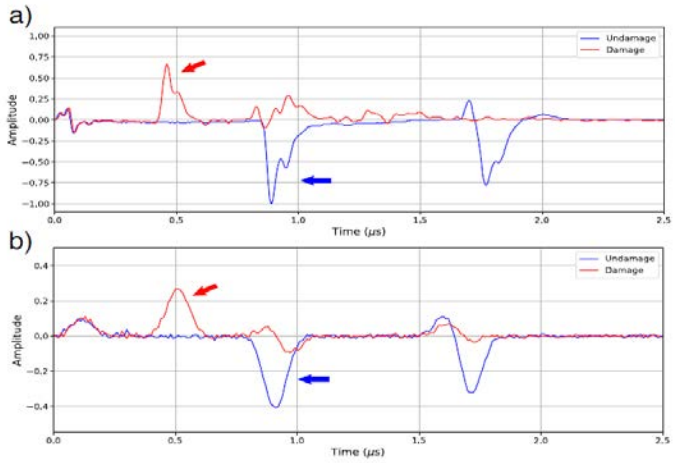


**Figure 8: TDR pulse responses from the coaxial cable with the short termination. a. Numerical modeling of the TDR response with and without damage. b. Experimental TDR response of the coaxial cable with and without damage. The red curve is the response from the damaged coaxial cable, whereas the blue curve is from un-damaged cable.**

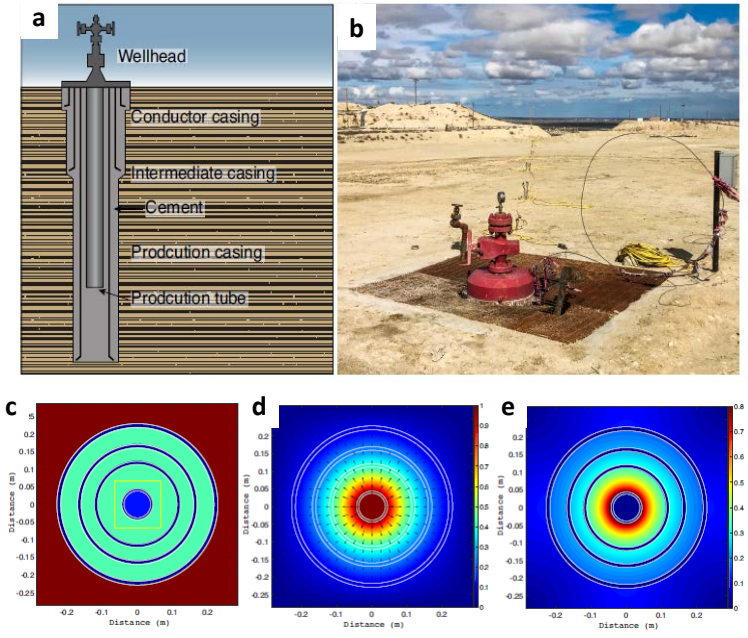


**Figure 9: a. Schematic diagram of the experimental well; b. Photograph of the wellhead; c. Cross-section of the numerical modeling of the well; Dark blue rings are the casings. Light blue is the fluid (oil) inside the well. Cyan represents the cementation formation. The yellow box in the middle is the contour for the Gauss integration in Equation 4; d. Normalized voltage potential field. The black arrows represent electric field direction; e. Normalized electric field.**

Both the numerical simulation and the experimental observation of the reflectometry signals are shown in Figure 10. As shown in Figure 10b, a clear reflected signal from the end of casing was observed. The slight mismatch of the timing of the reflected signals between the experimental data and the numerical signal (Figure 10a) is due to the simplified velocity model used in the numerical simulations by disregarding the variation of the geology in the vertical profile. We also note the multiple reflections along the signal trace, which are likely a result of the multiple interactions and reflections between the different casing layers. Regardless, this results provide the first-ever field evidence of this technology for its applications in deep, complicated boreholes. More tests using a range of such boreholes, including some with known damages, are underway to better characterize the signals and its linkage with the damage state of these casings.

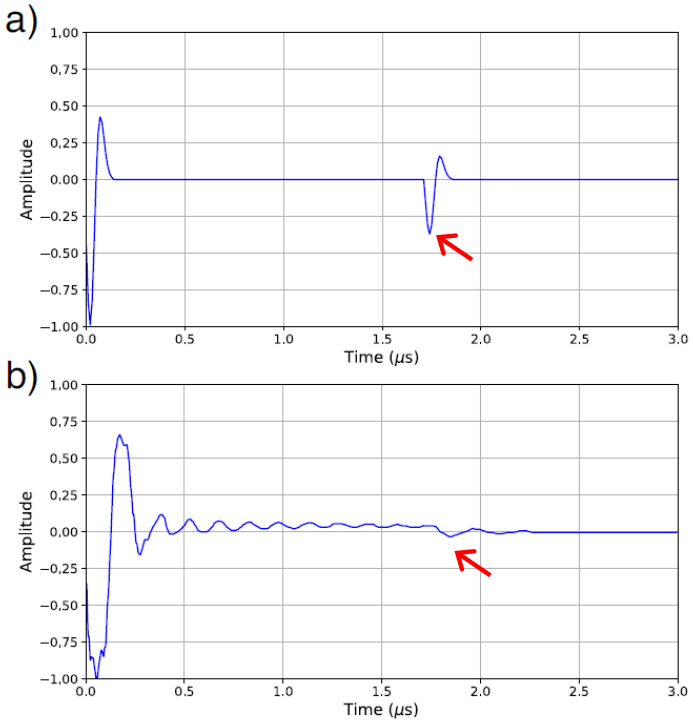


**Figure 10: TDR pulse responses from the 1D numerical modeling and the field experiment at the experimental well. a. Numerical modeling of the TDR response; b. TDR response observed from the well in the field. Red arrows indicate the reflections from the bottom of the casing.**

### *3.3 Seismic Tube wave*

In addition to EM reflectometry, seismic tube wave method was also tested for its application in borehole integrity monitoring. As discussed above, this method is similar to the EM reflectometry method and relies on the reflection of the seismic tube wave in responding to borehole integrity issues, such as damage or break-off.

Figure 11 shows a numerical simulation of the tube wave on a borehole with multiple layers of cements as shown in Figure 11a. The simulation is based on a well in the same field for the EM reflectometry tests shown above. Figure 11b and 11c shows the characteristics of the tube waves at time stamps 0.07s and 0.2s. As can be seen from the figure, multiple reflections from the

cement/formation interfaces lead to a very complex wave pattern near the wellbore and challenges the identification of the wave signals from the borehole itself.

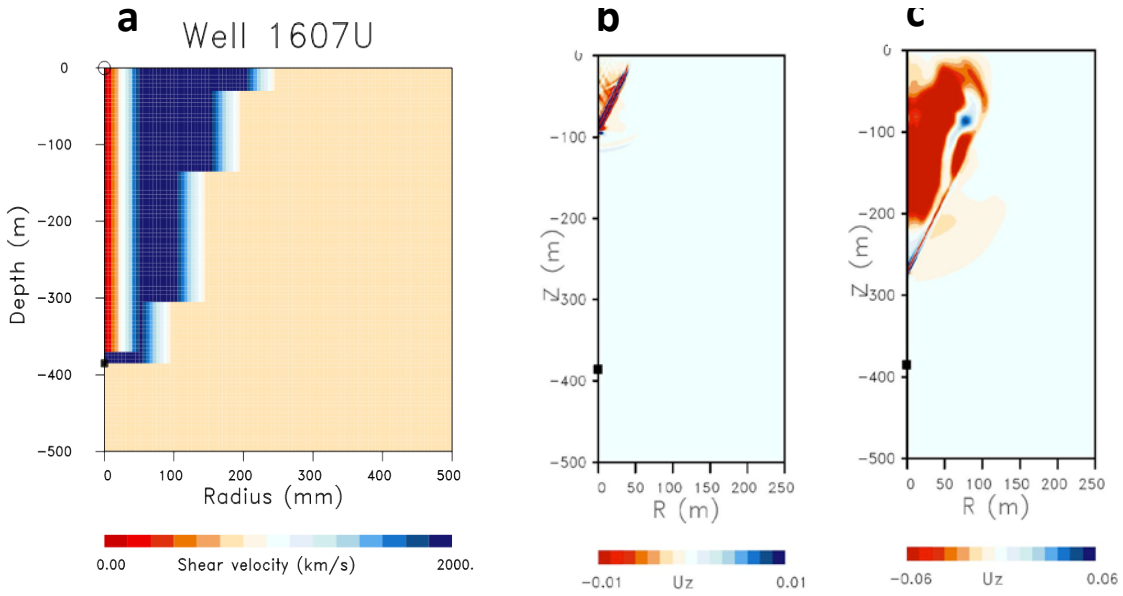


**Figure 11: a. Casing seismic velocity model used for tube wave simulation; b. Tube wave near the casing at 0.07s after excitation; c. Tube wave at 0.2s after excitation.**

Experimental tests of the tube wave method were conducted in the field following the diagram shown in Figure 12. The wellbore is roughly 650m deep and does not have known severe damages, therefore the major reflection is expected to occur at the bottom. Both 3-component geophone and an array of single component geophone array were used in the experiments to capture the signals near the wellhead. Based on the data shown in Figure 12b/12c, potential reflections from the bottom of the casing were identified in both types of geophones. Specifically, all three components (x, y, z) of the Episensor geophone show clear reflection at ~ 1.45 second, which is consistent with the realistic velocity model at the site. Such a signal is also visible on the traces of the single component geophone arrays showing a trend following the distances of the geophones from the closest to the furthest.

## 4. Conclusion

New methods for fast and economic borehole integrity diagnosis is lacking. The technologies presented in this study demonstrated the significant potentials of a set of novel methods for the diagnosis of damages to any steel based boreholes in the subsurface. Specifically, both the steady state and transient EM approaches as well as the seismic tube wave methods have been tested with successful results at numerical, laboratory and field scales, demonstrating the feasibility of the technologies for wellbore integrity monitoring.

Based on what we have learned, additional critical research and testing needs include further study to specifically link signal characteristics to the degree of borehole damages, the identification of a range of boreholes at field scales to test the applicability of these tools in a variety of subsurface applications, development of integration strategies to jointly utilize the different signals as well as the joint application testing with federal and industry partners for further developments.

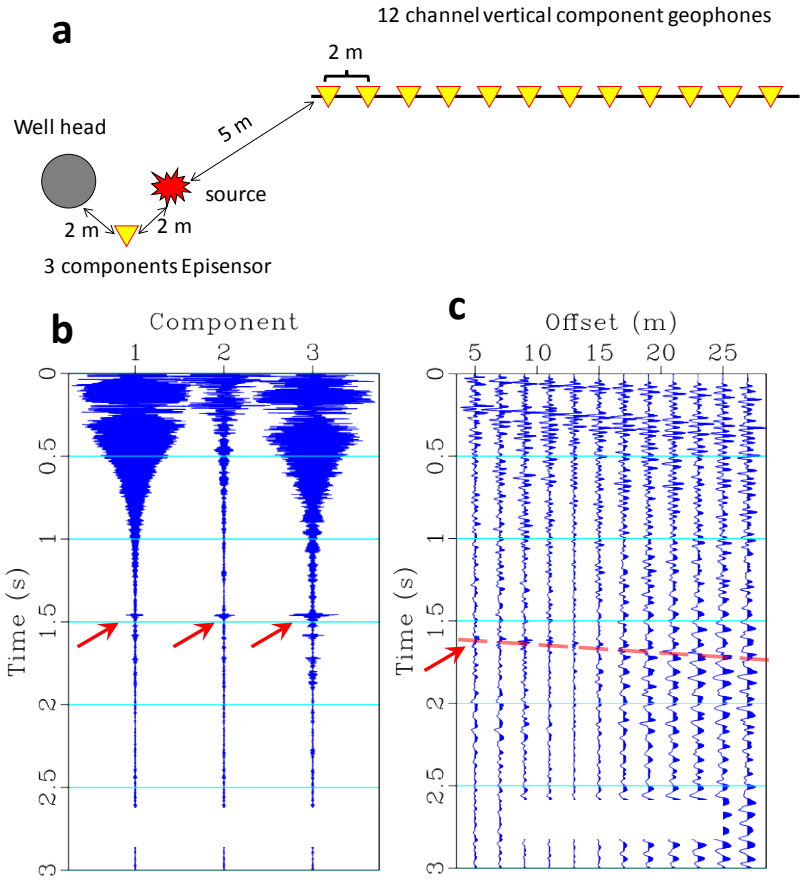


**Figure 12: a. Field experimental layout for seismic tube wave experiment; b. Seismic traces from the x, y, z components of the geophone.; c. Seismic traces recorded on the single component geophones. The red arrows indicate the identified tube wave reflection**

## Acknowledgement

The authors wish to thank the Geothermal Technologies Office at the Department of Energy for providing funding for this research under the wellbore integrity topic. We also thank Chevron Corporation for providing access to the test wells. This research used resources of the National Energy Research Scientific Computing Center (NERSC), a U.S. Department of Energy Office of Science User Facility operated under Contract No. DE-AC02-05CH11231. The authors wish to acknowledge the contributions of Lawrence Berkeley National Laboratory's Geosciences Measurement Facility (GMF) for custom instrumentation solutions for our field experiments.

## REFERENCES

Alexandrov, D.V., A. Bakulin, S. Ziatdinov, 2007, Reflection and transimission of tube waves in cased boreholes with layers and perforations, SEG Technical program expended abstract, 10.1190/1.2793118

Amir, N., O. Barzelay, A. Yefet, T. Pechter, 2010, Condenser tube examination using acoustic pulse reflectometry, Journal of Engineering for Gas Turbines and Power, Vol.132, 014501-1

Furse, C., P. Smith, M. Diamond, 2009, Feasibility of reflectometry for nondestructive evaluation of prestressed concrete anchors, IEEE Sensors Journal, Vol. 9, No. 11, p1322-1329

Lasia, A., 2014, Electrochemical Impedance Spectroscopy and its Applications, Springer, New York.

Ledieu J., Ridder P.D., De Clerck P., Dautrebande S., 1986, A method of measuring soil moisture by time-domain reflectometry, J. Hydro. V 88, 3–4, p319-328.

Ponomarenko, A., 2008, The tube wave reflection from borehole fracture, JASS8, Sate University St. Petersburg.

Schenkel, C.J., and H.F. Morrison, 1990, Effects of well casing on potential field measurements using downhole current sources, Geophysical Prospecting, Vol. 38, p663-686

Schenkel, C.J., and H.F. Morrison, 1994, Electrical resistivity measurement through metal casing, Geophysics, Vol. 59, No.7, p1072-1082

Commer, M., M. Hoversten, E. Um, 2015, Transient-electromagnetic finite-difference time-domain earth modeling over steel infrastructure, Geophysics, 2015, 80(2), E147-E162.

Um, E., M. Commer, G. A Newman, and M. Hoversten, Finite element modelling of transient electromagnetic fields near steel-cased wells, Geophysical Journal International, 202(2), 903-913.

Weiss, C J, 2017, Finite element analysis for model parameters distributed on a hiearchy of geometric simplices, Geophysics, v82, doi: 10.1190/GEO2017-0058.1

Wilt, M., G. Nieuwenhuis, K. Maclennan and E. Um, 2018, Casing-integrity mapping using top-casing electrodes and surface based EM fields, SEG Technical Program Expanded Abstracts, p858-862.

Wilt, M., E. Um, E. Nichols, C. Weiss, K. Maclennan and G. Nieuwenhuis, 2019, Casing Integrity Mapping using Top-Casing Electrodes and Surface Based Electromagnetic Fields, submitted to Geophysics after the revision and currently under review.